Inorganic Chemistry

Article

pubs.acs.org/IC

Tracking of Tuning Effects in Bis-Cyclometalated Iridium Complexes: A Combined Time Resolved Infrared Spectroscopy, Electrochemical, and Computational Study

Danielle N. Chirdon,[†] Catherine E. McCusker,[‡] Felix N. Castellano,*[,‡] and Stefan Bernhard*[,†]

[†]Department of Chemistry, Carnegie Mellon University, Pittsburgh, Pennsylvania 15213, United States

[‡]Department of Chemistry and Center for Photochemical Sciences, Bowling Green State University, Bowling Green, Ohio 43403, United States

Supporting Information

ABSTRACT: Electronic structure and photophysical properties have been investigated for a new series of fluorinated iridium complexes with the parent $[Ir(ppy)_2(deeb)](PF_6)$ (deeb is 4,4′-diethylester-2,2′-bipyridine). Time resolved infrared spectroscopy (TRIR) has been used to observe the long-lived triplet excited state of each complex confirming its mixed charge transfer character. Supplementary evidence of charge transfer in the triplet state is provided via emission spectroscopy, transient absorption spectroscopy, and density functional theory (DFT) calculations. Both computational and spectroscopic assignments reveal consistency in the first excitation throughout the series of complexes. Electrochemical measurements meanwhile show that increasing fluorination still induces expected shifting of frontier orbitals. Excited states beyond the lowest lying triplet are probed for the complexes via UV−vis spectroscopy which reveals three distinct features. These features are assigned via time-dependent DFT (TD-DFT) to build a broader understanding of electronic structure.

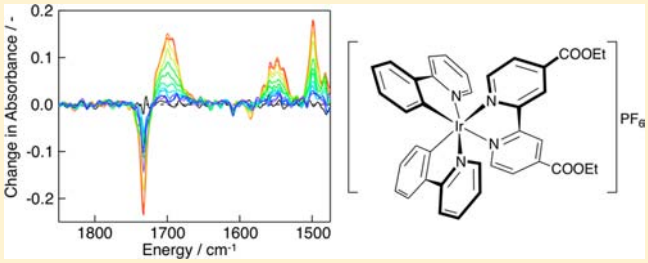

INTRODUCTION

Cyclometalated iridium(III) complexes play vital roles in contemporary lighting, alternative energy, and biological research. These complexes form a diverse and efficient class of emitters for organic light emitting diodes[1−3] and light emitting electrochemical cells.[4,5] They are also leading catalysts for light-driven hydrogen reduction,[1,6] and their use as emissive probes has elucidated biological interactions.[7,8]

The popularity of iridium(III) complexes for practical applications stems largely from their tunable, triplet excited state. Strong spin orbit coupling from the iridium allows for efficient intersystem crossing from the first singlet excited state to the triplet manifold. For many cyclometalated iridium complexes, metal to ligand charge transfer (MLCT) and ligand based triplet states are so similar in energy that the first triplet excited state is a linear combination of both.[9,10] Thus, electrons are effectively promoted from a highest occupied molecular orbital (HOMO) with both metal d and ligand π character to a ligand π^* orbital.[11] Involvement of ligand orbitals in both the HOMO and the lowest unoccupied molecular orbital (LUMO) ensures that the energies of those levels and the associated HOMO−LUMO gap are readily controlled through rational ligand design.[12−14] For iridium complexes containing one diimine ancillary ligand and two cyclometalating phenylpyridine ligands, the phenylpyridine's phenyl ring often contributes π orbitals to the HOMO[6] whereas the ancillary ligand is primarily involved with the LUMO.[3,15] The first transition thus resembles a MLCT/interligand charge transfer,[15] and the main effect of adding electron withdrawing groups to the phenyl ring is HOMO stabilization which blue shifts the photoluminescence.[3,9] Addition of electron donating groups to the diimine ligand also produces a blue-shifted emission spectrum but does so through LUMO destabilization.[3,16] By combining modifications of the ancillary and cyclometalating ligands, Lowry et al. have observed emission across the visible spectrum in complexes of the form $[Ir(C^N)_2(N^N)]$ (C^N = cyclometalating ligand and N^N = neutral bidentate ancillary ligand).[14]

Despite successful application of ligand modifications, various investigations suggest that this tuning strategy produces effects beyond simple adjustment of frontier orbital energies. For iridium phenylpyridine complexes, detailed computation has shown that the addition of electron withdrawing groups to stabilize the HOMO may also redistribute the LUMO.[17] Meanwhile, analysis of nonradiative decay constants has introduced the possibility of a shift in the excitation from MLCT to intraligand transfer across a series of cyclometalated complexes.[10] Shifting of excited state character has also been suggested for a different set of complexes by time-resolved photoluminescence spectroscopy. Using this latter technique, alteration of the ancillary ligand has been shown to induce

Received: April 23, 2013
Published: July 11, 2013

   dx.doi.org/10.1021/ic401009q | *Inorg. Chem.* 2013, 52, 8795−8804

quenching of an initial MLCT emissive state by a second excited state believed to be a new interligand charge transfer.[18]

Complete understanding of the effects of tuning is necessary to design molecules not only with specific emissive properties but also with appropriate orbital placement for functions including charge injection. Time resolved infrared spectroscopy (TRIR) is a promising tool for furthering current understanding by monitoring the nature of the excited state and energy transitions within emission tuned complexes. Vibrational bands observed in infrared spectroscopy are highly dependent on electron density distribution.[19] Thus, TRIR detects any electron transfer during excitation as dramatic shifting of the ground state vibrational bands. Furthermore, vibrational bands are functional group specific, so detected shifts are associated with precise portions of the sample molelcule.[20] In iridium complexes, this direct association can identify the ligands where charge transfer occurs, thereby revealing the "location" of the excited state.

In the past, TRIR spectroscopy on inorganic complexes has largely been restricted to chromophores containing C≡O and C≡N$^-$ ligands with large oscillator strengths and frequencies compatible with appropriate solvent windows.[19,21] However, TRIR sensitivity continues to improve, and moderate intensity carbonyl (C═O) stretches have now been exploited to track the MLCT excited state of ruthenium bipyridine complexes having one ester substituted ligand.[20] Carbonyl and acetylene IR stretches have also been employed as tags for direct observation of ligand localized and charge transfer excited states in Pt(II) complexes.[22,23]

Here, a multifaceted approach involving TRIR is employed to probe the result of increasing phenylpyridine modification in three new [Ir(C^N)$_2$(deeb)](PF$_6$) complexes (deeb is 4,4′-diethylester-2,2′-bipyridine). A similar series of cyclometalated iridium complexes has previously been investigated by Hanss et al. through a combination of photoluminescence spectroscopy and electrochemistry. This investigation suggests that fluorination of the phenylpyridine ligand shifts the character of the complex's electronic transition from MLCT to LC.[24] However, direct evidence of the transition's specific features is not provided, and some observations including dramatic alteration of emission lifetimes and quantum efficiencies by ester substitution of the ancillary ligand cannot be fully rationalized. For the series of materials prepared here, TRIR results are used with other spectroscopic evidence to conclusively demonstrate that the emissive state remains consistent despite tuning. All spectroscopic assignments are further verified by computations while electrochemical analysis is used to reveal that tuning still changes the frontier orbital energies.

EXPERIMENTAL SECTION

General Information. Phenylpyridine, $IrCl_3{\cdot}4H_2O$, and all reaction solvents were used as received from commercial sources. Fluorinated phenylpyridine ligands were accessed via Kröhnke and Suzuki pathways described previously.[6] Cyclometalated chloro-bridged iridium dimers were also synthesized by literature procedures using ethoxyethanol instead of methoxyethanol in the solvent mixture.[14] The neutral ligand 4,4′-diethylester-2,2′-bipyridine (deeb) was obtained from commercial 2,2′-bipyridine-4,4′-dicarboxylic acid through the method of Hales and Beattie.[25]

^{13}C and ^{1}H NMR spectra were recorded on a Bruker Avance 500 MHz spectrometer at room temperature. Molecular weights were determined from acetonitrile solutions with a Thermo-Fisher Finnigan LCQ instrument using an electrospray ionization source.

Synthesis of [Ir(ppy)$_2$(deeb)](PF$_6$). Bis-(μ)-chlorotetrakis(2-phenyl-pyridinato-C^2,N)diiridium(III) (0.092 mmol, 0.099 g) was stirred with deeb (0.213 mmol, 0.064 g) in refluxing ethanol (4 mL, 190 proof) open to the air. After 68 h, the reaction mixture was cooled to room temperature, combined with D.I. water (50 mL), and extracted with diethyl ether (3 × 60 mL). Residual ether was removed from the aqueous layer via gentle heating, and ammonium hexafluorophosphate (1.00 g) was added in minimal water to precipitate product. Precipitation was facilitated by several hours of cooling, and the resulting orange solid was collected via vacuum filtration. This product was recrystallized from acetonitrile through diffusion of ether vapor. Yield: 56.3%. ^{1}H NMR (acetone-d$_6$, 500 MHz): δ 9.33 (d, 2H, J = 0.900 Hz, deeb-H^3), 8.33 (d, 2H, J = 5.55 Hz, deeb-H^6), 8.25 (d, 2H, J = 8.10 Hz, ppy, pyridyl-H^3), 8.17 (dd, 2H, J = 5.65, 1.60 Hz, deeb-H^5), 7.97 (m, 2H, ppy, pyridyl-H^4), 7.92 (dd, 2H, J = 7.83, 0.875 Hz, ppy, phenyl-H^3), 7.89 (d, 2H, J = 5.80 Hz, ppy, pyridyl-H^6), 7.13 (m, 2H, ppy, pyridyl-H^5), 7.06 (td, 2H, J = 7.56, 1.13 Hz, ppy, phenyl-H^4), 6.94 (td, 2H, J = 7.45, 1.25 Hz, ppy, phenyl-H^5), 6.34 (dd, 2H, J = 7.58, 0.625 Hz, ppy, phenyl-H^6), 4.48 (q, 4H, J = 7.12 Hz, deeb-CH$_2$), 1.40 (t, 6H, J = 7.1269 Hz, deeb-CH$_3$). ^{13}C NMR (acetone-d$_6$, 500 MHz): δ 168.49, 164.10, 157.61, 152.81, 150.52, 150.42, 144.86, 141.42, 139.81, 132.44, 131.42, 128.95, 125.95, 125.37, 124.61, 123.75, 120.97, 63.41, 14.40. LRMS (m/z; ESI): 801.2 (100%, M- PF$_6$). HRMS calculated for $C_{38}H_{32}N_4O_4Ir$, 799.2029; Found, 799.2026.

Synthesis of [Ir(F-mppy)$_2$(deeb)](PF$_6$). Reaction conditions for [Ir(ppy)$_2$(deeb)](PF$_6$) were employed again using bis-(μ)-chlorotetrakis(5-methyl-2-(4-fluorophenyl)-pyridinato-C^2,N)-diiridium(III) instead of the phenylpyridine variant of the iridium dimer. The purification process described above was also repeated except that the product was recrystallized from acetone: pentane rather than acetonitrile: ether and was collected as red crystals. Yield: 79.3%. ^{1}H NMR (acetone-d$_6$, 500 MHz): δ 9.30 (d, 2H, J = 0.950 Hz, deeb-H^3), 8.36 (dd, 2H, J = 5.60, 0.350 Hz, deeb-H^6), 8.16 (dd, 2H, J = 5.63, 1.62 Hz, deeb-H^5), 8.13 (d, 2H, J = 8.40 Hz, F-mppy, pyridyl-H^3), 7.96 (dd, 2H, J = 8.65, 5.60 Hz, F-mppy, phenyl-H^3), 7.83 (dd, 2H, J = 8.40, 1.30 Hz, F-mppy, pyridyl-H^4), 7.70 (s, 2H, F-mppy, pyridyl-H^6), 6.83 (td, 2H, J = 8.86, 2.58 Hz, F-mppy, phenyl-H^4), 5.93 (dd, 2H, J = 9.50, 2.60 Hz, F-mppy, phenyl-H^6), 4.49 (q, 4H, J = 7.10 Hz, deeb-CH$_2$), 2.10 (s, 6H, F-mppy, CH$_3$), 1.41 (t, 6H, J = 7.13, deeb-CH$_3$). ^{13}C NMR (acetone-d$_6$, 500 MHz): δ 165.31, 164.70, 164.08, 163.31, 157.56, 152.95, 152.92, 152.87, 149.74, 141.48, 141.02, 135.09, 128.98, 127.70, 127.63, 125.46, 120.66, 118.46, 118.31, 110.80, 110.62, 63.46, 17.86, 14.40. LRMS (m/z; ESI): 865.2 (100%, M- PF$_6$). HRMS calculated for $C_{40}H_{34}N_4O_4F_2Ir$, 863.2154; Found, 863.2147.

Synthesis of [Ir(dF(CF$_3$)ppy)$_2$(deeb)](PF$_6$). Bis-(μ)-chlorotetrakis(5-trifluoromethyl-2-(4,6-difluorophenyl)-pyridinato-C^2,N)diiridium(III) (0.0838 mmol, 0.125 g) and deeb (0.180 mmol, 0.054g) were stirred open to the air in refluxing ethanol (3.8 mL, 190 proof) for 25 h. The reaction mixture was then cooled to room temperature and poured into D. I. water (50 mL). Precipitated iridium complex was collected through vacuum filtration. Minimal acetone was used to redissolve the solid, and ammonium hexafluorophosphate (0.543 g) was added to the acetone solution in minimal water. Precipitation of the desired hexafluorophosphate salt from the acetone solution was forced by addition of water (10 mL) and subsequent removal of the acetone under reduced pressure. Yellow product was collected through vacuum filtration and recrystallized by acetone: pentane vapor diffusion. Yield: 52.7% (0.102 g). ^{1}H NMR (acetone-d$_6$, 500 MHz): δ 9.37 (d, 2H, J = 0.850 Hz, deeb-H^3), 8.63 (dd, 2H, J = 8.80, 2.15 Hz, dF(CF$_3$)ppy, pyridyl-H^3), 8.52 (d, 2H, J = 5.60 Hz, deeb-H^6), 8.41 (dd, 2H, J = 8.78, 1.50 Hz, dF(CF$_3$)ppy, pyridyl-H^4), 8.19 (dd, 2H, J = 5.60, 1.55 Hz, deeb-H^5), 8.09 (s, 2H, dF(CF$_3$)ppy, pyridyl-H^6), 6.89 (m, 2H, dF(CF$_3$)ppy, phenyl-H^4), 5.96 (dd, 2H, J = 8.40, 2.25 Hz, dF(CF$_3$)ppy, phenyl-H^6), 4.49 (q, 4H, J = 7.12 Hz, deeb-CH$_2$), 1.40 (t, 6H, J = 7.10 Hz, deeb-CH$_3$). ^{13}C NMR (acetone-d$_6$, 500 MHz): δ 168.56, 168.50, 166.65, 166.54, 164.59, 164.57, 164.49, 164.47, 164.00, 162.49, 162.38, 157.70, 155.23, 155.17, 153.89, 147.72, 147.68, 147.64, 147.60, 142.30, 138.63, 129.46, 127.90, 126.82, 126.54, 126.06, 125.17, 125.00, 124.19, 122.03, 115.70, 115.67, 115.55,

dx.doi.org/10.1021/ic401009q | Inorg. Chem. 2013, 52, 8795−8804

115.53, 100.95, 100.73, 100.52, 63.73, 14.48. LRMS (m/z; ESI): 1009.2 (100%, M- PF_6). HRMS calculated for $C_{40}H_{26}N_4O_4F_{10}Ir$, 1007.1400; Found, 1007.1398.

Electrochemistry. Cyclic voltammograms were collected using a CH-Instruments Electrochemical Analyzer 600C potentiostat with a three electrode system consisting of a 1 mm^2 platinum disk working electrode, a coiled platinum counter electrode, and a silver wire reference electrode. Potential scans were performed at 100 mV/s under an argon purge in acetonitrile solutions containing 0.10 M tetrabutylammonium hexafluorophosphate and 0.8−1.0 mM sample complex. An internal ferrocene standard was added to each solution, and potentials were referenced to SCE by setting the ferrocene oxidation to 0.40 V.[26]

Steady-State Spectroscopy. All photophysical measurements were performed in spectrophotometric grade dichloromethane (DCM) in 1 cm^2 quartz cells unless otherwise stated. Prior to measurement, samples were deoxygenated by either sparging with argon for 20 min or freeze−pump−thaw degassing for three cycles. Absorption spectra were acquired using a Cary 50 spectrophotometer. Steady state emission spectra were collected with a FL/FS920 fluorometer (Edinburgh Instruments) equipped with a 450 W Xe arc lamp and a Peltier cooled, red sensitive PMT (R2658P Hamamatsu). Low temperature spectra were collected using an Optistat-DN optical cryostat and ITC-503 temperature controller (Oxford Instruments). Measurements were taken in 2-methyltetrahydrofuran (2-MeTHF) at 77 K after equilibrating for at least 30 min. Absolute quantum yields for the complexes were recorded with a Hamamatsu absolute quantum yield spectrometer (C11347). Optically dilute (OD = 0.1−0.2) solutions were excited into the lowest energy absorption feature (530 nm for $[Ir(ppy)_2(deeb)](PF_6)$ and $[Ir(F\text{-}mppy)_2(deeb)](PF_6)$ and 475 nm for $[Ir(dF(CF_3)ppy)_2(deeb)](PF_6)$), and reported values are the average of 6 measurements. The Parker−Rees correction was used when converting the spectra to an energy scale.[27]

Transient Absorption and Photoluminescence Spectroscopy. Single wavelength kinetic decays and total time-resolved spectra in both photoluminescence and transient absorption experiments were collected with an LP920 laser flash photolysis system (Edinburgh Instruments). The excitation source was the Vibrant LD 355 II Nd:YAG/OPO system (OPOTEK). Data acquisition was controlled by the LP900 software program (Edinburgh Instruments). Samples were prepared in spectrophotometric grade DCM, with an optical density of 0.1−0.2 at the excitation wavelength for emission measurements and 0.3−0.5 at the excitation wavelength for transient absorption measurements. Kinetic traces were collected with a PMT (R928 Hamamatsu), and transient absorption difference spectra were collected with an iStar ICCD camera (Andor Technology). Kinetic traces were adequately fit using single exponential functions in IGOR Pro. Samples showed no evidence of decomposition as ascertained by UV−vis experiments performed before and after each acquisition.

Time Resolved Infrared Spectroscopy. Nanosecond time-resolved step−scan FT-IR absorption spectra were measured on a step−scan-modified Bruker Vertex 70 FT-IR spectrometer which has been described previously.[22] Briefly, solutions were prepared in spectrophotometric grade DCM to give a ground-state infrared absorption of 0.4−0.7 for the carbonyl band (~12 mM) and degassed with argon for 20 min. Spectra were measured in a 0.2 mm demountable CaF_2 cell (Specac). $[Ir(ppy)_2(deeb)](PF_6)$ and $[Ir(F\text{-}mppy)_2(deeb)](PF_6)$ were excited using the 532 nm second-harmonic output of a Nd:YAG laser (Continuum Surelite I) (~8 mJ/pulse, ~2 cm diameter spot, 10 Hz). $[Ir(dF(CF_3)ppy)_2(deeb)](PF_6)$ was excited at 450 nm (~10 mJ/pulse, ~2 cm diameter spot, 10 Hz) using the OPO coupled output of a Nd:YAG laser (Continuum Surelite I). The AC signal from the PV-MCT detector was amplified (10 or 20 X) with a 100 MHz fast preamplifier (FEMTO DHPVA). The interferogram response before and after laser excitation was collected in 10 ns time slices, with 20 ($[Ir(ppy)_2(deeb)](PF_6)$ and $[Ir(F\text{-}mppy)_2(deeb)](PF_6)$) or 30 ($[Ir(dF(CF_3)ppy)_2(deeb)](PF_6)$) laser shots averaged at each mirror position. Long- and short-pass filters (Spectragon) were used to isolate the spectral region of interest. For each scan, folding limits of 2400 and 1300 cm^{-1} and 4 cm^{-1} resolution resulted in 614 mirror positions. The reported differential absorption spectra are an average of 10 scans, and ground-state spectra are an average of 32 (rapid) scans. Samples showed no significant evidence of decomposition as ascertained by FT-IR spectra measured before and after each time-resolved data acquisition. Ground state spectra were fit with Lorentzian peaks using the multipeak fitting function in IGOR Pro.

Density Functional Theory (DFT) Calculations. Calculations on the three complexes were performed using the Gaussian 09 software package[28] and the computational resources of the Ohio Supercomputer Center. Geometry optimizations were performed on both the ground state and the lowest energy triplet state using the unrestricted B3LYP functional, the 6-31g(d) basis set on all nonmetal atoms, and the LANL2DZ basis set on the Ir atom.[29−31] The polarizable continuum model (PCM) was used to simulate the effects of the dichloromethane solvent environment for all calculations. Frequency calculations were also performed on all optimized structures. No imaginary frequencies were obtained for any of the optimized geometries. For comparison to experimental values, the calculated frequencies were scaled by a factor of 0.9613, the reported correction factor for the B3LYP/6-31g(d) functional and basis set.[22,32]

Time-Dependent DFT (TD-DFT). Time dependent calculations were performed at the optimized ground-state geometry via Gaussian 09 software. Symmetry was restricted to C_2, and the PCM was employed to simulate CH_2Cl_2 solvent effects. The unrestricted B3LYP functional was used, and the LANL2DZ basis set was applied to all atoms since that basis set has previously resulted in superior agreement of TD-DFT spectra with experimental data.[33] The energy, oscillator strength, and rotatory strength were computed for each of the 70 lowest singlet excitations. Involved orbitals were visualized using Molekel[34] while UV−vis spectra were generated from the singlet excitations with GaussSum 2.0.[35] Electronic transitions were expanded as Gaussian curves with a fwhm (full width at half- maximum) for each peak set to 0.37 eV.

RESULTS AND DISCUSSION

Synthesis. All three iridium complexes investigated here (Figure 1) were synthesized in two steps adapted from a literature procedure.[14] Briefly, the cyclometalating phenylpyridine was added to $IrCl_3{\cdot}4H_2O$ to form a dichloro-bridged dimer which was then cleaved through addition of the ancillary ligand 4,4′-diethylester-2,2′-bipyridine (deeb). This process was carried out entirely in ethanol and ethoxyethanol to prevent transesterification of the deeb's ethyl ester substituent. The final isolated products were structurally characterized by ^1H and ^{13}C NMR along with mass spectrometry.

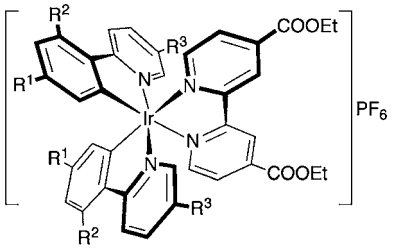

$[Ir(ppy)_2(deeb)](PF_6)$: R^1, R^2, R^3=-H
$[Ir(F\text{-}mppy)_2(deeb)](PF_6)$: R^1=-F, R^2=-H, R^3=-CH_3
$[Ir(dF(CF_3)ppy)_2(deeb)](PF_6)$: R^1, R^2=-F, R^3=-CF_3

Figure 1. Cyclometalated iridium(III) complexes used to study the effects of tuning.

Electrochemistry. Electrochemical measurements were collected for the iridium complexes to study the influence of tuning and deeb's ester functionality on redox chemistry (Table 1, Figure 2). Reversible oxidations are observed for [Ir-

dx.doi.org/10.1021/ic401009q | Inorg. Chem. 2013, 52, 8795−8804

Table 1. Electrochemical Potentials

compound	E_{ox} (V vs SCE)[a]	ΔE (mV)	E_{red} (V vs SCE)[a]	ΔE (mV)
$[Ir(ppy)_2(deeb)](PF_6)$	1.33	80	−1.00, −1.54	66, 67
$[Ir(F\text{-}mppy)_2(deeb)](PF_6)$	1.46	76	−0.98, −1.52	67, 63
$[Ir(dF(CF3)ppy)_2(deeb)](PF_6)$			−0.88, −1.40	65, 68

[a]Potentials measured in degassed acetonitrile solution.

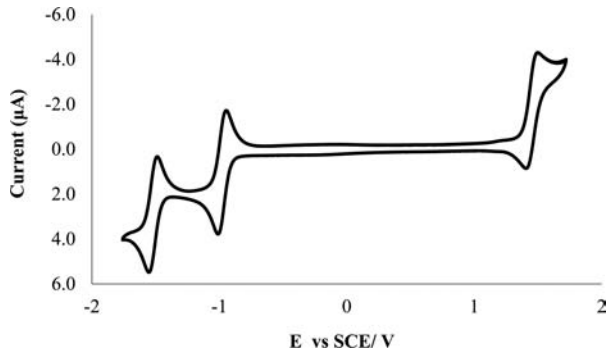

Figure 2. Cyclic voltammogram of $[Ir(F\text{-}mppy)_2(deeb)](PF_6)$ which is representative of the redox features witnessed for the entire series of cyclometalated iridium complexes. The voltammogram was collected in 0.10 M TBAH/ACN solution, and potentials were adjusted to SCE based on a ferrocene standard ($E_{fc/fc+}$ = +0.40 V).

$(ppy)_2(deeb)](PF_6)$ and $[Ir(F\text{-}mppy)_2(deeb)](PF_6)$. Observed oxidations are assigned to removal of electrons from an iridium-centered HOMO with possible contributions from phenylpyridine π orbitals. All three complexes show two reversible reductions. The first reduction is assigned to deeb based on the reduction observed for that ligand in $[Ru(deeb)_3]^{2+}$.[36] The second reduction meanwhile corresponds to placement of an electron in a phenylpyridine π^* orbital.[6]

The electron withdrawing effect of the ethyl ester in deeb is evident in the ease of deeb's reduction in $[Ir(ppy)_2(deeb)](PF_6)$ (−1.00 V vs SCE) as compared to the more difficult reduction of the ancillary bipyridine in $[Ir(ppy)_2(bpy)](PF_6)$ (−1.41 V vs SCE).[37] Electron deficiency in deeb also draws electron density away from the iridium center shifting the oxidation in the parent complex to a slightly more positive potential than is observed for $[Ir(ppy)_2(bpy)](PF_6)$ (1.24 V vs SCE).[37] A similar effect is seen for the phenylpyridine reduction and brings it within the solvent window for each compound even though phenylpyridine reduction is often not observed for cyclometalated Ir materials.[6]

Within the series of iridium complexes, increasing fluorination of the phenylpyridine ligand shifts all redox processes to more positive potentials. Oxidation dramatically shifts by +0.13 V upon addition of one fluorine to ppy and then is no longer observed in $[Ir(dF(CF_3)ppy)_2(bpy)](PF_6)$, which signals further shifting beyond the positive limit of the solvent window (~1.69 V). Consistent, significant increases in the difficulty of oxidation occur since fluorination of ppy can stabilize the HOMO directly via two possible methods: participation of the ppy in the HOMO itself and reduced sigma donation to the metal center. Such electron withdrawal from the metal is also expected to indirectly reduce electron density at the deeb-centered LUMO facilitating deeb's reduction. This reduction is only negligibly effected by initial ppy fluorination suggesting that the added electron deficiency is not sufficient for establishing a widespread indirect effect. The lack of change also reflects the sporadic nature of indirect electrochemical effects which has been observed previously.[6] Further ppy fluorination ultimately establishes the expected inductive withdrawal from deeb giving a substantial anodic shift of its reduction. The pattern in deeb's reduction potentials is closely mimicked by ppy's reduction potentials since the ease of ppy reduction depends not only on the stabilization of ppy but also on stabilization of the negative charge resulting from the preceding reduction. Cyclic voltammograms for each compound are available in the Supporting Information.

Infrared Spectroscopy. The ground state infrared spectra of the three iridium complexes in CH_2Cl_2 solution are presented in Figure 3 with $Ir(ppy)_3$ and $[Ru(deeb)_3]^{2+}$ spectra.

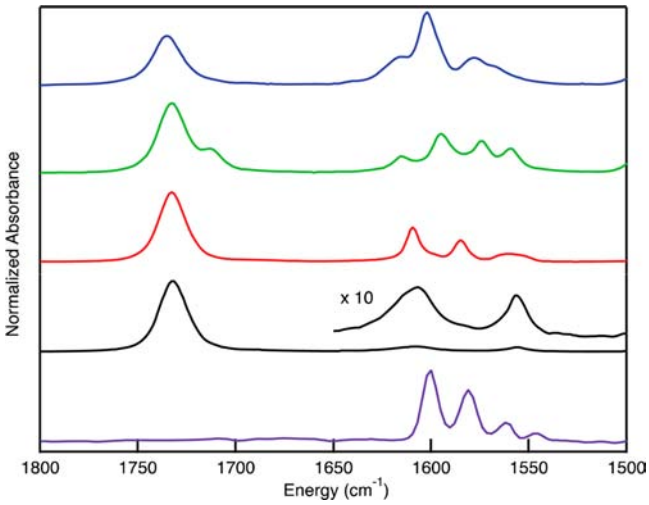

Figure 3. Normalized ground state infrared absorption spectra of $Ir(ppy)_3$ (purple), $[Ru(deeb)_3](PF_6)_2$ (black), $[Ir(ppy)_2(deeb)](PF_6)$ (red), $[Ir(F\text{-}mppy)_2(deeb)](PF_6)$ (green), and $[Ir(dF(CF_3)\text{-}ppy)_2(deeb)](PF_6)$ (blue) in CH_2Cl_2 solutions, measured in a 0.2 mm path length CaF_2 cell.

The band around 1730 cm^{-1} corresponds to the C═O bond stretch of the deeb ligand. Within this absorption envelope, there are two closely spaced infrared allowed C═O bond stretching vibrations assuming C_2 symmetry: the in-phase combination (a symmetry mode) and the out-of-phase combination (b symmetry mode). In the ring stretching region of the spectrum (1630−1500 cm^{-1}), contributions are made by both the deeb and ppy ligands, but based on comparison to the spectra of $[Ru(deeb)_3]^{2+}$ and $Ir(ppy)_3$, the intensity of the deeb contribution is much less than that of the ppy ligand. The overlapping absorption features in this region were deconvolved into four distinct peaks by Lorentzian fitting (see Supporting Information).

Cyclometalated Ir complexes have been previously studied by infrared and Raman spectroscopy,[38] but not to the same level of detail as $[Ru(bpy)_3]^{2+}$ and related complexes.[39] Thus, to gain further insight into the four bands of the ring stretching region, the ground state vibrational spectra of the three complexes were calculated using Gaussian 09. The results of those calculations in comparison to the experimental absorption maxima can be seen in Table 2. The frequency calculations suggest that the four ring stretching signals are due to four types of ligand vibrations: the highest energy band

dx.doi.org/10.1021/ic401009q | Inorg. Chem. 2013, 52, 8795−8804

Table 2. Ground State Infrared Spectra

$[Ir(ppy)_2(deeb)](PF_6)$			$[Ir(F\text{-}mppy)_2(deeb)](PF_6)$			$[Ir(dF(CF_3)ppy)_2(deeb)](PF_6)$		
exp[a]	DFT[b]	type[c]	exp[a]	DFT[b]	type[c]	exp[a]	DFT[b]	type[c]
1732.8	1721.9	$\nu(C{=}O)_b$	1732.8	1722.2	$\nu(C{=}O)_b$	1735.2	1723.5	$\nu(C{=}O)_b$
	1722.4	$\nu(C{=}O)_a$		1722.7	$\nu(C{=}O)_a$		1724.0	$\nu(C{=}O)_a$
1609.4	1597.3	ν(py)	1615.3	1603.7	ν(py)	1618.2	1608.4	ν(py)
1584.9	1575.0	ν(ph)	1594.5	1575.2	ν(ph)	1601.7	1579.0	ν(ph)
1562.3	1556.6	ν(ppy)	1574.4	1558.6	ν(ppy)	1578.1	1555.1	ν(ppy)
1554.6	1551.7	ν(deeb)	1559.0	1551.9	ν(deeb)	1567.5	1552.3	ν(deeb)
	1543.5	ν(ppy)		1546.8	ν(ppy)		1549.3	ν(ppy)

[a]Maxima of the experimental infrared spectra, collected in CH_2Cl_2 solution in a 0.2 mm path length CaF_2 cell. Maxima from 1650 to 1500 cm^{-1} are the result of a multipeak fitting analysis, where the spectra were fit with 4 Lorentzian peaks. [b]Selected ground state frequencies calculated using UB3LYP and 6-31g(d) on C, H, N, and O and LANL2DZ on Ir scaled by 0.9613. [c]Types of vibrations: $\nu(C{=}O)_b$ is the b symmetry carbonyl stretch, $\nu(C{=}O)_a$ is the a symmetry carbonyl stretch, ν(py) is the ring stretch of the pyridyl half of ppy, ν(ph) the ring stretch of the phenyl half of ppy, ν(deeb) is the ring stretch of the bipyridine ligand, and ν(ppy) is the ring stretch of the entire ppy ligand.

represents stretching of the pyridyl ring in ppy (ν(py)), the next highest band represents stretching of ppy's phenyl ring (ν(ph)), the third peak has contributions from stretching of deeb (ν(deeb)) as well as the entire ppy ligand (ν(ppy)), and the lowest energy peak is due to the stretching of the entire ppy ligand (ν(ppy)). The calculations show that the energies of ppy-based vibrations slightly increase with fluorination. This is in agreement with the trend in the Lorentzian fits of the experimental data.

The TRIR difference spectrum of $[Ir(ppy)_2(deeb)](PF_6)$ is compared to the ground state spectrum in Figure 4 and Table 3. The difference spectrum shows that both the carbonyl stretching vibration and the group of ring stretching vibrations shift to lower energy upon excitation. The carbonyl absorption peak shifts to lower energy by ~35 cm^{-1}, consistent with a reduction in the C=O bond order. These results indicate an Ir-to-deeb MLCT excited state since an MLCT excitation formally reduces deeb by promoting an electron into its π^* antibonding orbital which weakens the conjugated C=O bonds. Moreover, the shift observed in the carbonyl stretch is similar to those reported for ruthenium and rhenium complexes possessing metal-to-deeb charge transfer excited states.[40,41]

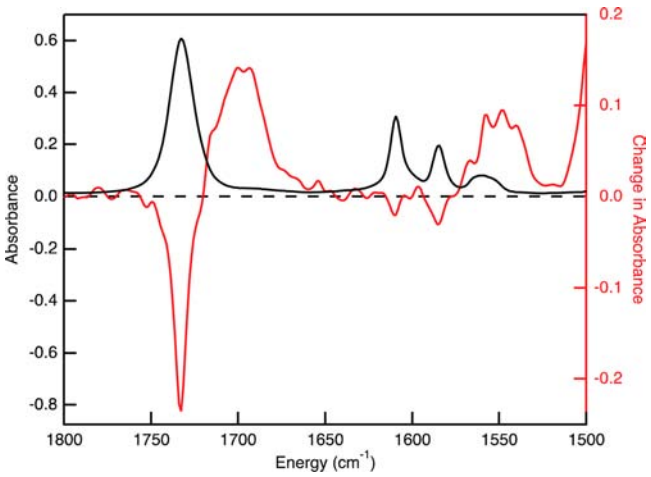

Figure 4. Comparison between the measured TRIR difference spectrum 20 ns after 532 nm excitation (red) and the ground state absorption spectrum (black) for $[Ir(ppy)_2(deeb)](PF_6)$.

For the ring stretching vibrations, there is not a simple one-to-one correlation between ground state features and the observed maximum in the TRIR difference spectrum. Resolution of the transient spectrum is too low for individual contributions to be extracted from the broad excited state absorption band. However, in general, the ring stretching vibrations are clearly shifted to lower energy in the excited state. For the deeb stretching vibrations, this shift can be explained in the same manner as the shift in the C=O stretch: population of a π^* antibonding orbital in the MLCT excited state weakens the C=C and C=N bonds of the deeb ligand and shifts their stretching frequency to lower energy. The reason for the shift in the ppy stretching frequencies is less intuitive. As suggested previously, the MLCT excited state of cyclometalated iridium(III) complexes is often more accurately described as a combination of metal-to-ligand and ligand-to-ligand charge transfer. Significant covalent interaction between the Ir(III) and phenyl ring of the cyclometalating ppy ligand causes the HOMO (singlet)/LSOMO (triplet) orbitals to be significantly delocalized over the ppy as shown in Figure 5. As a result, upon excitation, electron density is removed from the π

Table 3. SSIR Results[a]

	$[Ir(ppy)_2(deeb)](PF_6)$			$[Ir(F\text{-}mppy)_2(deeb)](PF_6)$			$[Ir(dF(CF_3)ppy)_2(deeb)](PF_6)$		
	GS	SSIR	ΔE	GS	SSIR	ΔE	GS	SSIR	ΔE
C=O	1733	1696	−37	1733	1698	−35	1735	1710	−25
ring[b]	1609	~1548	−61 to −6	1615	~1547	−68 to −12	1618	~1548	−70 to −20
	1585			1595			1602		
	1562			1574			1578		
	1554			1559			1568		

[a]Maxima of the experimental infrared spectra, collected in CH_2Cl_2 solution in a 0.2 mm path length CaF_2 cell. GS is the ground state spectrum, SSIR is the time-resolved step scan IR spectra, and ΔE = SSIR-GS. [b]Reported GS maxima are the result of a multipeak fitting analysis, where the experimental spectra from 1650 to 1500 cm^{-1} were fit with 4 Lorentzian peaks.

dx.doi.org/10.1021/ic401009q | Inorg. Chem. 2013, 52, 8795−8804

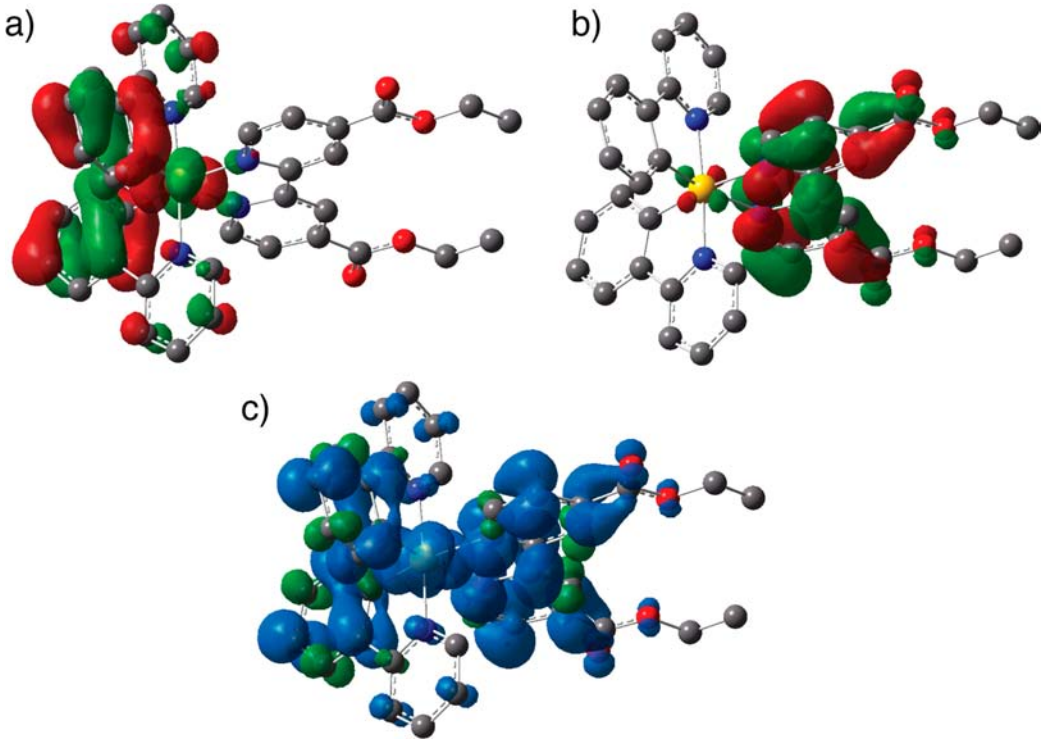

Figure 5. Calculated (a) LSOMO, (b) HSOMO, and (c) spin density for the lowest lying triplet state of $[Ir(ppy)_2(deeb)](PF_6)$.

Table 4. Calculated Singlet and Triplet Infrared Spectra[a]

$Ir(ppy)_2(deeb)](PF_6)$				$[Ir(F\text{-}mppy)_2(deeb)](PF_6)$				$Ir(dF(CF_3)ppy)_2(deeb)](PF_6)$			
singlet	triplet	ΔE[b]	type[c]	singlet	triplet	ΔE	type	singlet	triplet	ΔE	type
1722.4	1690.1	−32.3	$\nu(C{=}O)_a$	1722.7	1690.4	−32.3	$\nu(C{=}O)_a$	1724.0	1693.2	−30.8	$\nu(C{=}O)_a$
1721.9	1679.9	−42.0	$\nu(C{=}O)_b$	1722.2	1680.3	−41.9	$\nu(C{=}O)_b$	1723.5	1684.0	−39.5	$\nu(C{=}O)_b$
1597.3	1594.7	−2.6	ν(py)	1603.7	1593.4	−10.1	ν(py)	1608.4	1606.1	−2.3	ν(py)
1575.0	1540.7	−34.3	ν(ph)	1575.2	1519.6	−55.6	ν(ph)	1579.0	1544.1	−34.9	ν(ph)
1556.6	1560.6	+4	ν(ppy)	1558.6	1556.1	−2.5	ν(ppy)	1555.1	*d*	*d*	ν(ppy)
1551.7	1528.9	−22.8	ν(deeb)	1551.9	1529.0	−22.9	ν(deeb)	1552.3	1532.1	−20.2	ν(deeb)

[a]Calculated frequencies of the lowest energy singlet and triplet states, scaled by 0.9613. Spectra were calculated from the optimized singlet and triplet geometries in a dichloromethane solvent continuum, using the UB3LYP functional and the 6-31g(d) basis set on all nonmetal atoms and the LANL2DZ basis set on the Ir atoms. [b]ΔE = Triplet-Singlet. [c]Types of vibrations: $\nu(C{=}O)_a$ is the a symmetry carbonyl stretch, $\nu(C{=}O)_b$ is the b symmetry carbonyl stretch, ν(py) is the ring stretch of the pyridyl half of the ppy ligand, ν(ph) the ring stretch of the phenyl half of the ppy ligand, ν(deeb) is the ring stretch of the bipyridine ligand, and ν(ppy) is the ring stretch of the entire ppy ligand. [d]No peak corresponding to a ppy vibration in the range of 1800−1500 cm^{-1}.

bonding orbitals of the ppy ligands weakening the C=C bonds and causing a net lowering of their vibrational frequencies. Spin density calculations for the parent compound (Figure 5c) further illustrate the loss of an electron from a metal-ppy orbital by showing that unpaired spins generated in the charge transfer triplet excited state are located not only on the deeb and metal but also on the ppy.

The calculated vibrational spectra of the ground state and lowest energy triplet states (Supporting Information, Figures S6−S8) were generated to understand the origin of the excited state shifts, particularly in the ring-stretching region. In the carbonyl region of $[Ir(ppy)_2(deeb)](PF_6)$, the calculated carbonyl bands shift to lower energy, with the in-phase (a) mode shifting by ∼30 cm^{-1} and the out-of-phase (b) mode shifting by ∼40 cm^{-1} (Table 4). This difference in shifting has been observed in other 4,4′-substituted bipyridine complexes[20b] and explains the broadening of the excited state C=O absorption relative to the ground state. In the ring stretching region, the calculated ν(deeb) vibration shifts to lower energy by about 20 cm^{-1} indicating deeb's possible participation in the broad excited state feature shifted by −61 to −6 cm^{-1} in the experimental spectrum. For the ppy ligand, there is very little change in calculated ν(py) or ν(ppy), but ν(ph) shifts to lower energy by almost 35 cm^{-1} suggesting that it also contributes to the experimental excited state band. The discrepancy in the calculated shifts of ν(py) and ν(ph) can be understood from the LSOMO in Figure 5. That orbital which is an admixture of Ir and phenyl character shows only limited involvement of the pyridyl half of the ppy ligand. Therefore, in the charge transfer excited state, more electron density is removed from the phenyl ring than the pyridyl ring leading to a larger shift for ν(ph).

Comparison of the TRIR difference spectra for all three of the complexes shows very little difference (Figure 6). In particular, the magnitude of the red shift in the carbonyl stretching frequency, which is relatively well-defined, is similar for all three molecules. This strongly suggests that for [Ir(F-

dx.doi.org/10.1021/ic401009q | Inorg. Chem. 2013, 52, 8795−8804

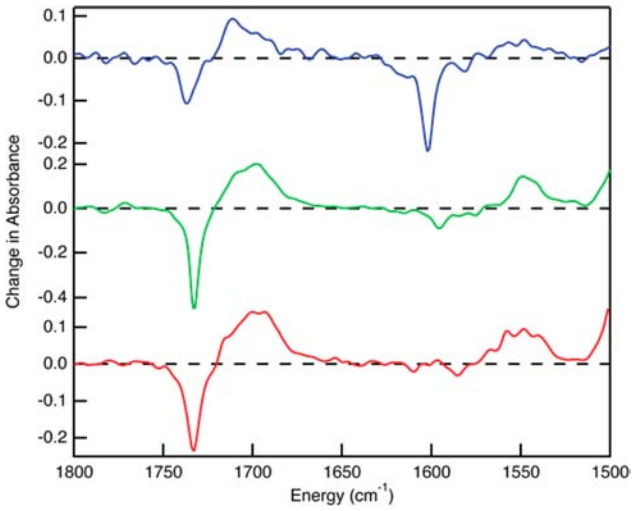

Figure 6. Time resolved SSIR difference spectra of $[Ir(ppy)_2(deeb)](PF_6)$ (red, λ_{ex} = 532 nm), $[Ir(F\text{-}mppy)_2(deeb)](PF_6)$ (green, λ_{ex} = 532 nm), and $[Ir(dF(CF_3)ppy)_2(deeb)](PF_6)$ (blue, λ_{ex} = 450 nm) 20 ns after laser excitation.

mppy)$_2$(deeb)](PF$_6$) and [Ir(dF(CF$_3$)ppy)$_2$(deeb)](PF$_6$), the nature of the long-lived excited state is the same as that in [Ir(ppy)$_2$(deeb)](PF$_6$): mixed metal-to-ligand/ligand-to-ligand charge transfer rather than ligand centered.

Emission and Transient Absorbance Spectroscopy. Room temperature steady state emission spectra (Figure 7) are broad and featureless for all three complexes. Emission maxima range from 680 nm for [Ir(ppy)$_2$(deeb)](PF$_6$) to 564 nm for [Ir(dF(CF$_3$)ppy)$_2$(deeb)](PF$_6$) showing that the energy of the long-lived excited state increases with increasing degree of fluorination (Table 5). The blue shift of the emission indicates that HOMO stabilization already seen in electrochemical

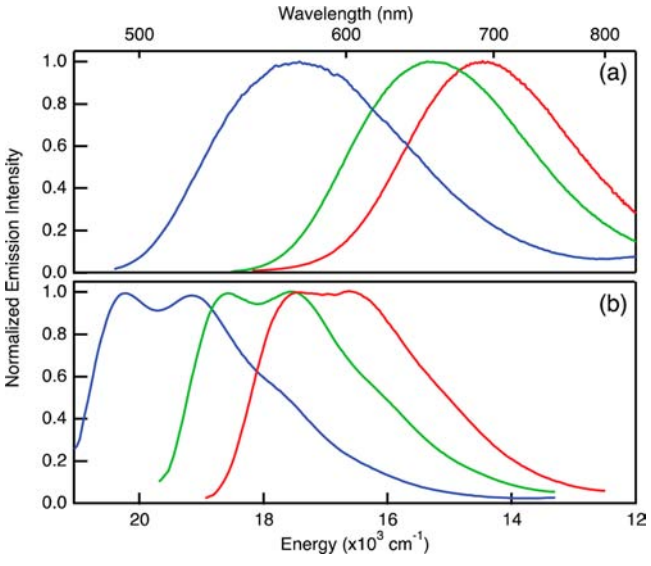

Figure 7. Normalized steady state emission spectra of [Ir(ppy)$_2$(deeb)](PF$_6$) (red), [Ir(F-mppy)$_2$(deeb)](PF$_6$) (green), and [Ir(dF(CF$_3$)ppy)$_2$(deeb)](PF$_6$) (blue) measured after excitation into the lowest energy CT bands (530 nm for [Ir(ppy)$_2$(deeb)](PF$_6$) and [Ir(F-mppy)$_2$(deeb)](PF$_6$) and 480 nm for [Ir(dF(CF$_3$)ppy)$_2$(deeb)](PF$_6$)) in (a) deoxygenated DCM solution at room temperature, and (b) deoxygenated 2-Me-THF glass at 77 K. Spectra are corrected for instrumental response.

measurements is a dominant effect of phenylpyridine fluorination. In 2-MeTHF low temperature glasses at 77 K, the spectra of all three complexes shift to higher energy (2500–3000 cm^{-1}) and become more structured, characteristic of a high charge transfer component in the emissive state.[42] The similarity of the three spectra at room temperature and low temperature suggests that the emissive state is the same for all three complexes: a charge transfer state. This corroborates the TRIR findings. The emission peaks however cannot provide the same detailed insight into the roles of each ligand in the long-lived emissive state which are detected via TRIR and allow for specific assignment of the state.

Along with the increase in emission energy across the series, there is also an increase in both the emission quantum yield and lifetime going from 5.2% and 115 ns for [Ir(ppy)$_2$(deeb)](PF$_6$) to a remarkable 79.5% and 1145 ns for [Ir(dF(CF$_3$)-ppy)$_2$(deeb)](PF$_6$). Further analysis shows a modest increase in the radiative decay rate as the emission energy increases. The large increase in quantum yield and lifetime across the series is primarily reflected in the large decrease in the nonradiative rate across the series as the emission energy increases. This trend is consistent with the predictions of the energy gap law for a single excited state.

Pulsed laser excitation (5–7 ns fwhm) into the lowest energy absorption bands of the three compounds generated absorption transients possessing single exponential decay kinetics quantitatively identical to those observed in the time-resolved photoluminescence experiments (Supporting Information, Figure S9). The transient absorption difference spectra of the three complexes were also recorded at room temperature (RT) and are displayed in Figure 8. The three transient absorbance spectra are strikingly similar suggesting that the same type of excited state is produced in each instance. They each possess a sharp absorption feature near 400 nm as well as weaker, broader absorption features in the midvisible region (~450–550 nm). This spectral shape particularly the sharp feature at 400 nm has been observed in many [Ir(ppy)$_2$(N^N)]$^+$ (N^N is a diimine ligand) complexes and is characteristic of charge transfer terminating on the diimine ligand.[43] The spectrum is also consistent with the absorption features of the free deeb radical anion.[36] As with emission, transient absorption results are in agreement with assignment of the long-lived excited state in all three complexes as an Ir(ppy)-to-deeb charge transfer state.

Electronic Spectroscopy. The UV–vis spectra of the complexes all show three distinct features: a high energy, high intensity excitation with a shoulder band (I), a moderately intense transition (II), and a very weak, low energy transition (III). Increasing fluorination in the complexes shifts II and III to higher energies, and in [Ir(dF(CF$_3$)ppy)$_2$(deeb)](PF$_6$), this causes II to overlap with feature I (Figure 9).

Time dependent DFT calculations were performed for [Ir(ppy)$_2$(deeb)](PF$_6$) and [Ir(dF(CF$_3$)ppy)$_2$(deeb)](PF$_6$) to elucidate the observed transitions. These calculations underestimate the intensity of transition III in [Ir(ppy)$_2$(deeb)](PF$_6$) (Figure 10) since the experimental intensity can be bolstered by a theoretically forbidden singlet to triplet transition enabled by spin–orbit coupling.[44] Otherwise, the calculated spectrum is in excellent agreement with the three features observed experimentally. Feature I which would conventionally be attributed to intraligand $\pi\rightarrow\pi^*$ transitions[15] can be partly assigned to such transitions for [Ir(ppy)$_2$(deeb)](PF$_6$) but also involves promotion from orbitals with metal and metal-phenyl

dx.doi.org/10.1021/ic401009q | Inorg. Chem. 2013, 52, 8795–8804

Table 5. Photophysical Properties of Studied Complexes

compound	λ_{Em} (nm) RT[a]	λ_{Em} (nm) 77 K[b]	Φ_{Em} (%)[a,c]	τ_{obs} (ns)[a,d]	k_r ($\times 10^5$ s^{-1})[a]	k_{nr} ($\times 10^5$ s^{-1})[a]
$[Ir(ppy)_2(deeb)](PF_6)$	680	571	5.2	115 ± 5	4.52	82.4
$[Ir(F\text{-}mppy)_2(deeb)](PF_6)$	644	537	19.3	390 ± 15	4.95	20.7
$[Ir(dF(CF_3)ppy)_2(deeb)](PF_6)$	564	493	79.5	1145 ± 40	6.94	1.79

[a]Measurements in deoxygenated DCM at room temperature. [b]Measurements in deoxygenated 2-Me-THF at 77 K. [c]Average of 6 absolute quantum yield measurements accurate to ±2% relative. [d]Average excited state lifetimes from time-resolved emission and transient absorption experiments.

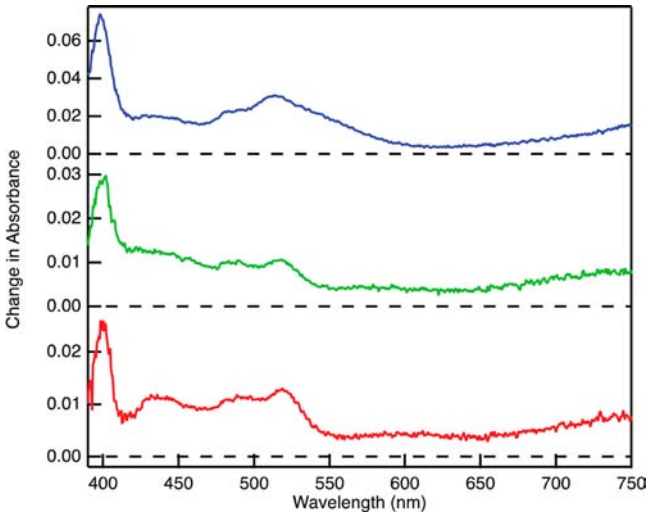

Figure 8. Transient absorption difference spectra of $[Ir(ppy)_2(deeb)](PF_6)$ (red, λ_{ex} = 532 nm), $[Ir(F\text{-}mppy)_2(deeb)](PF_6)$ (green, λ_{ex} = 532 nm), and $[Ir(dF(CF_3)ppy)_2(deeb)](PF_6)$ (blue, λ_{ex} = 450 nm) measured in deoxygenated DCM solution.

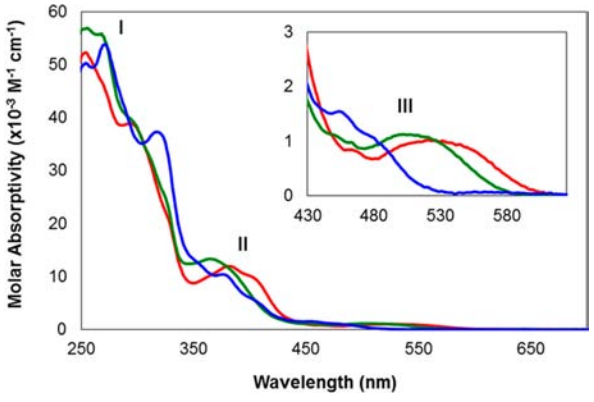

Figure 9. UV−vis absorbance spectra of $[Ir(ppy)_2(deeb)](PF_6)$ (red), $[Ir(F\text{-}mppy)_2(deeb)](PF_6)$ (green), and $[Ir(dF(CF_3)ppy)_2(deeb)](PF_6)$ (blue) measured in DCM solution at room temperature. The low energy portion of the spectra is enlarged in the inset to show details of the weakest transition.

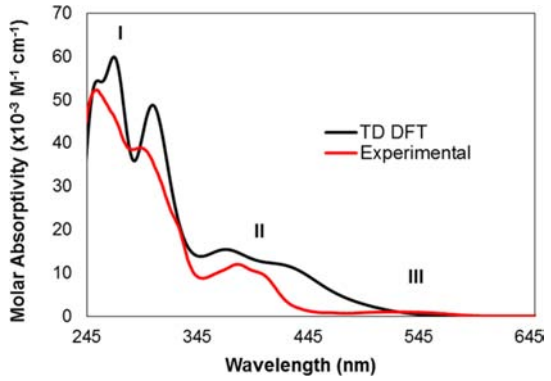

Figure 10. Experimental (red) and calculated (black) UV−vis absorbance spectra for $[Ir(ppy)_2(deeb)](PF_6)$. The calculated spectrum was generated via time dependent DFT calculations with Gaussian[28] and GaussSum software.[35].

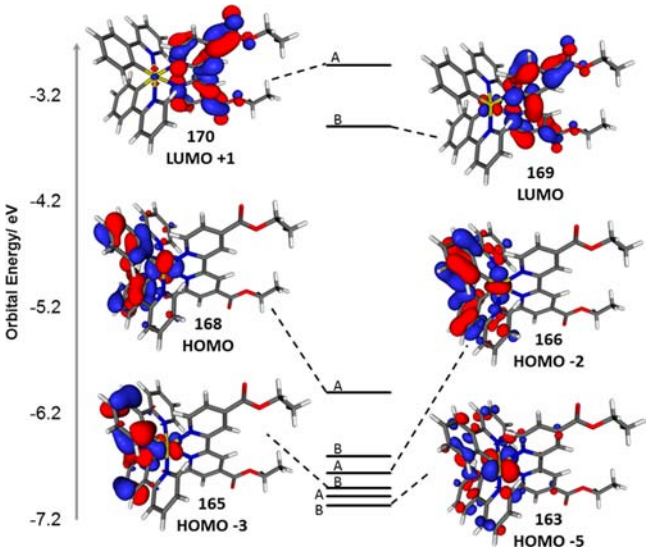

Figure 11. Frontier orbital diagram constructed for $[Ir(ppy)_2(deeb)](PF_6)$ from the TD-DFT calculations. C_2 symmetry labels are provided for the orbitals.

bonding character. Meanwhile, transition II in the calculations for the parent clearly results from mixed MLCT/ligand-to-ligand charge transfers. It encompasses excitation from orbitals 163, 164, 165, and 166 which consist of metal d orbitals in nonbonding or slightly bonding interactions with phenyl π orbitals (Figure 11). All of these excitations terminate on the deeb centered LUMO (169) or LUMO+1 (170). Transition III is also a MLCT/ligand-to-ligand transfer, but it is lower in energy because it represents excitation across the complex's energy gap from the HOMO which is destabilized relative to 163−165 by metal-phenylpyridine antibonding character. The TD-DFT assignment of the HOMO−LUMO transition is consistent with observations of the lowest lying excited state in $[Ir(ppy)_2(deeb)](PF_6)$ via TRIR and the other spectroscopic techniques. Details of all calculated transitions for $[Ir(ppy)_2(deeb)](PF_6)$ are available in the Supporting Information with the calculated spectrum and transitions for $[Ir(dF(CF_3)ppy)_2(deeb)](PF_6)$.

The electronic structure of $[Ir(dF(CF_3)ppy)_2(deeb)](PF_6)$ established from TD-DFT calculations is very similar to that of $[Ir(ppy)_2(deeb)](PF_6)$ except for the presence of a lower lying

dx.doi.org/10.1021/ic401009q | Inorg. Chem. 2013, 52, 8795−8804

ppy π^* orbital (LUMO+3). Thus, the calculated HOMO−LUMO transition is left unchanged by fluorination as expected from spectroscopic findings. In fact, the only appreciable difference in the transitions of the fluorinated derivative $[Ir(dF(CF_3)ppy)_2(deeb)](PF_6)$ and the parent is increased phenylpyridine $\pi\rightarrow\pi^*$ character in transition II of the former.

CONCLUSIONS

A family of three bis-cyclometalated deeb complexes has been synthesized, and a multifaceted approach has been used to determine the complete effect of ligand tuning on their electronic structure. Cyclic voltammetry reveals that increasing the degree of fluorination of the two 2-phenylpyridine units leads to an expected stabilization of the electrochemical HOMO and LUMO. The luminescence maximum was blue-shifted by over 120 nm upon introduction of fluoro-substituents showing HOMO stabilization to be a dominant effect. Meanwhile, emission quantum yields and lifetime measurements reveal a 10-fold increase. Emission and transient absorption spectra are both consistent with a mixed MLCT/ligand-to-ligand transfer excited state for all complexes. TRIR further confirms the consistent nature of excitation throughout the series and directly shows the expected transfer of charge to deeb upon excitation. All spectroscopic findings are supported by static DFT calculations while time dependent calculations provide more detail about the electronic structure of the increasingly electro-deficient complexes. In the future, TRIR may be employed either with other spectroscopic techniques or where such tools are ineffective to better understand tuning in a variety of iridium materials.

ASSOCIATED CONTENT

Supporting Information

Cyclic voltammograms and time-resolved emission decays are provided for all complexes along with calculated infrared vibrational frequencies and spectra. Detailed TD-DFT results are given including transition compositions, oscillator strengths, and the calculated electronic spectrum for $[Ir(dF(CF_3)ppy)_2(deeb)](PF_6)$. Lastly, NMR spectra and ground state IR Lorentzian fits are also provided. This material is available free of charge via the Internet at http://pubs.acs.org.

AUTHOR INFORMATION

Corresponding Author

*E-mail: castell@bgsu.edu (F.N.C.), bern@cmu.edu (S.B.).

Notes

The authors declare no competing financial interest.

ACKNOWLEDGMENTS

The CMU authors acknowledge support from the National Science Foundation through CHE-1055547 and the Princeton MRSEC Grant DMR-0819860. D.N.C. gratefully acknowledges the support of the U.S. Department of Energy Office of Science Graduate Research Fellowship. The BGSU portion of the work was supported by the Chemical Sciences, Geosciences and Biosciences Division, Office of Basic Energy Sciences, Office of Science, U.S. Department of Energy (DE-FG02-12ER16348). Additionally, the authors would like to thank Husain Kagalawala for synthesis of one of the iridium dimer precursors used here.

REFERENCES

(1) Ulbricht, C.; Beyer, B.; Friebe, C.; Winter, A.; Schubert, U. *Adv. Mater.* **2009**, *21*, 4418−4441.
(2) Xiao, L.; Chen, Z.; Qu, B.; Luo, J.; Kong, S.; Gong, Q.; Kido, J. *Adv. Mater.* **2011**, *23*, 926−952.
(3) Baranoff, E.; Yum, J.-H.; Graetzel, M.; Nazeeruddin, Md. K. *J. Organomet. Chem.* **2009**, *694*, 2661−2670.
(4) Bolink, H. J.; Cappelli, L.; Coronado, E.; Graetzel, M.; Orti, E.; Costa, R. D.; Viruela, P. M.; Nazeeruddin, Md. K. *J. Am. Chem. Soc.* **2006**, *128* (46), 14786−14787.
(5) Su, H.-C.; Fang, F.-C.; Hwu, T.-Y.; Hsieh, H.-H.; Chen, H.-F.; Lee, G.-H.; Peng, S.-M.; Wong, K.-T.; Wu, C.-C. *Adv. Funct. Mater.* **2007**, *17* (6), 1019−1027.
(6) Lowry, M. S.; Goldsmith, J. I.; Slinker, J. D.; Rohl, R.; Pascal, R. A., Jr.; Malliaras, G. G.; Bernhard, S. *Chem. Mater.* **2005**, *17*, 5712−5719.
(7) Lo, K. K.-W.; Zhang, K. Y.; Leung, S.-K.; Tang, M.-C. *Angew. Chem., Int. Ed.* **2008**, *47* (12), 2213−2216.
(8) Lo, K. K.-W.; Chung, C.-K.; Zhu, N. *Chem.—Eur. J.* **2006**, *12* (5), 1500−1512.
(9) Lowry, M. S.; Bernhard, S. *Chem.—Eur. J.* **2006**, *12*, 7970−7977.
(10) Flamigni, L.; Barbieri, A.; Sabatini, C.; Ventura, B.; Barigelletti, F. *Top. Curr. Chem.* **2007**, *281*, 143−203.
(11) Li, J.; Djurovich, P. I.; Alleyne, B. D.; Yousufuddin, M.; Ho, N. N.; Thomas, J. C.; Peters, J. C.; Bau, R.; Thompson, M. E. *Inorg. Chem.* **2005**, *44*, 1713−1727.
(12) Lamansky, S.; Djurovich, P.; Murphy, D.; Abdel-Razzaq, F.; Lee, H. E.; Adachi, C.; Burrows, P. E.; Forrest, S. R.; Thompson, M. E. *J. Am. Chem. Soc.* **2001**, *123* (18), 4304−4312.
(13) You, Y.; Park, S. Y. *J. Am. Chem. Soc.* **2005**, *127*, 12438−12439.
(14) Lowry, M. S.; Hudson, W. R.; Pascal, R. A., Jr.; Bernhard, S. *J. Am. Chem. Soc.* **2004**, *126*, 14129−14135.
(15) Bolink, H. J.; Cappelli, L.; Cheylan, S.; Coronado, E.; Costa, R. D.; Lardiès, N.; Nazeeruddin, Md. K.; Orti, E. *J. Mater. Chem.* **2007**, *17*, 5032−5041.
(16) Goldsmith, J. I.; Hudson, W. R.; Lowry, M. S.; Anderson, T. H.; Bernhard, S. *J. Am. Chem. Soc.* **2005**, *127* (20), 7502−7510.
(17) Zhou, G.; Ho, C.-L.; Wong, W.-Y.; Wang, Q.; Ma, D.; Wang, L.; Lin, Z.; Marder, T.; Beeby, A. *Adv. Funct. Mater.* **2008**, *18*, 499−511.
(18) You, Y.; Kim, K. S.; Ahn, T. K.; Kim, D.; Park, S. Y. *J. Phys. Chem. C* **2007**, *111*, 4052−4060.
(19) Schoonover, J. R.; Strouse, G. F. *Chem. Rev.* **1998**, *98*, 1335−1355.
(20) (a) Chen, P.; Omberg, K. M.; Kavaliunas, D. A.; Treadway, J. A.; Palmer, R. A.; Meyer, T. J. *Inorg. Chem.* **1997**, *36*, 954−955. (b) McCusker, C. E.; McCusker, J. K. *Inorg. Chem.* **2011**, *50*, 1656−1669.
(21) (a) Schoonover, J. R.; Gordon, K. C.; Argazzi, R.; Woodruff, W. H.; Bignozzi, C. A.; Dyer, R. B.; Meyer, T. J.; Peterson, K. A. *J. Am. Chem. Soc.* **1993**, *115*, 10996−10997. (b) Bridgewater, J. S.; Lee, B.; Bernhard, S.; Schoonover, J. R.; Ford, P. C. *Organometallics.* **1997**, *16*, 5592−5594.
(22) Prusakova, V.; McCusker, C. E.; Castellano, F. N. *Inorg. Chem.* **2012**, *51* (15), 8589−8598.
(23) Glik, E. A.; Kinayyigit, S.; Ronayne, K. L.; Towrie, M.; Sazanovich, I. V.; Weinstein, J. A.; Castellano, F. N. *Inorg. Chem.* **2008**, *47* (15), 6974−6983.
(24) Hanss, D.; Freys, J. C.; Bernardinelli, G.; Wenger, O. S. *Eur. J. Inorg. Chem.* **2009**, 4850−4859.
(25) Hales, N. J.; Beattie, J. F. *J. Med. Chem.* **1993**, *36*, 3853−3858.
(26) Connelly, N. G.; Geiger, W. E. *Chem. Rev.* **1996**, *96*, 877−910.
(27) Parker, C. A.; Rees, W. T. *Analyst (London)* **1960**, *85*, 587−600.
(28) Frisch, M. J.; Trucks, G. W.; Schlegel, H. B.; Scuseria, G. E.; Robb, M. A.; Cheeseman, J. R.; Scalmani, G.; Barone, V.; Mennucci, B.; Petersson, G. A.; Nakatsuji, H.; Caricato, M.; Li, X.; Hratchian, H. P.; Izmaylov, A. F.; Bloino, J.; Zheng, G.; Sonnenberg, J. L.; Hada, M.; Ehara, M.; Toyota, K. ; Fukuda, R.; Hasegawa, J.; Ishida, M.; Nakajima, T.; Honda, Y.; Kitao, O.; Nakai, H.; Vreven, T.; Montgomery, J. A. J.; Peralta, J. E.; Ogliaro, F. ; Bearpark, M.; Heyd, J. J.; Brothers, E.;

Kudin, K. N.; Staroverov, V. N.; Kobayashi, R.; Normand, J.; Raghavachari, K.; Rendell, A.; Burant, J. C.; Iyengar, S. S.; Tomasi, J.; Cossi, M.; Rega, N.; Millam, J. M.; Klene, M.; Knox, J. E.; Cross, J. B.; Bakken, V.; Adamo, C.; Jaramillo, J.; Gomperts, R. ; Stratmann, R. E.; Yazyev, O.; Austin, A. J.; Cammi, R.; Pomelli, C.; Ochterski, J. W.; Martin, R. L.; Morokuma, K.; Zakrzewski, V. G.; Voth, G. A.; Salvador, P.; Dannenberg, J. J.; Dapprich, S.; Daniels, A. D.; Farkas, O.; Foresman, J. B.; Ortiz, J. V.; Cioslowski, J.; Fox, D. J. *Gaussian 09*, revision A.01; Gaussian Inc.: Wallingford, CT, 2009.

(29) Dattelbaum, D. M.; Omberg, K. M.; Hay, P. J.; Gebhart, N. L.; Martin, R. L.; Schoonover, J. R.; Meyer, T. J. *J. Phys. Chem. A* **2004**, *108*, 3527−3536.

(30) Hua, F.; Kinayyigit, S.; Rachford, A. A.; Shikhova, E. A.; Goeb, S.; Cable, J. R.; Adams, C. J.; Kirschbaum, K.; Pinkerton, A. A.; Castellano, F. N. *Inorg. Chem.* **2007**, *46*, 8771−8783.

(31) Costa, R. D.; Céspedes-Guirao, F. J.; Bolink, H. J.; Fernández-Lázaro, F.; Sastre-Santos, Á.; Ortí, E.; Gierschner, J. *J. Phys. Chem. C* **2009**, *113*, 19292−19297.

(32) Scott, A. P.; Radom, L. *J. Phys. Chem.* **1996**, *100*, 16502−16513.

(33) Coughlin, F.; Westrol, M.; Oyler, K.; Byrne, N.; Kraml, C.; Zysman-Colman, E.; Lowry, M.; Bernhard, S. *Inorg. Chem.* **2008**, *47* (6), 2039−2048.

(34) Varetto, U. *Molekel*, 5.4.0.8; Swiss National Supercomputing Centre: Lugano, Switzerland.

(35) (a) O'Boyle, N. M. *GaussSum 2.0*; Dublin City University: Dublin, Ireland. 2006. Available at http://gaussum.sourceforge.net/. (b) O'Boyle, N. M.; Tenderholt, A. L.; Langner, K. M. *J. Comput. Chem.* **2008**, *29*, 839−845.

(36) Elliott, C. M.; Hershenhart, E. J. *J. Am. Chem. Soc.* **1982**, *104*, 7519−7526.

(37) Tinker, L. L.; Bernhard, S. *Inorg. Chem.* **2009**, *48*, 10507−10511.

(38) (a) Lai, S.-H.; Ling, J.-W.; Huang, Y.-M.; Huang, M.-J.; Cheng, C. H.; Chen, I.-C. *J. Raman Spectrosc.* **2011**, *42*, 332−338. (b) Tsai, H.-R.; Lu, K.-Y.; Lai, S.-H.; Fan, C.-H.; Cheng, C.-H.; Chen, I.-C. *J. Phys. Chem. C* **2011**, *115*, 17163−17174.

(39) (a) Mallick, P. K.; Danzer, G. D.; Strommen, D. P.; Kincaid, J. R. *J. Phys. Chem.* **1988**, *92*, 5628−5634. (b) Omberg, K. M.; Schoonover, J. R.; Treadway, J. A.; Leasure, R. M.; Dyer, R. B.; Meyer, T. J. *J. Am. Chem. Soc.* **1997**, *119*, 7013−7018. (c) Omberg, K. M.; Schoonover, J. R.; Bernhard, S.; Moss, J. A.; Treadway, J. A.; Kober, E. M.; Dyer, R. B.; Meyer, T. J. *Inorg. Chem.* **1998**, *37*, 3505−3508.

(40) Omberg, K. M.; Smith, G. D.; Kavaliunas, D. A.; Chen, P.; Treadway, J. A.; Schoonover, J. R.; Palmer, R. A.; Meyer, T. *J. Inorg. Chem.* **1999**, *38*, 951−956.

(41) Chen, P.; Palmer, R. A.; Meyer, T. J. *J. Phys. Chem. A* **1998**, *102*, 3042−3047.

(42) Tsuboyama, A.; Iwawaki, H.; Furugori, M.; Mukaide, T.; Kamatani, J.; Igawa, S.; Moriyama, T.; Miura, S.; Takiguchi, T.; Okada, S.; Hoshino, M.; Ueno, K. *J. Am. Chem. Soc.* **2003**, *125* (42), 12971−12979.

(43) Ichimura, K.; Kobayashi, T.; King, K. A.; Watts, R. J. *J. Phys. Chem.* **1987**, *91*, 6104−6106.

(44) Fantacci, S.; Angelis, F. D.; Wang, J.; Bernhard, S.; Selloni, A. *J. Am. Chem. Soc.* **2004**, *126*, 9715−9723.